J. Coat. Technol. Res., **14** (1) 95–106, 2017
DOI 10.1007/s11998-016-9844-y

Roll-to-roll gravure printing of thick-film silver electrode micropatterns for flexible printed circuit board

Kee-Hyun Shin, Ho Anh Duc Nguyen, Janghoon Park, Dongjun Shin, Dongjin Lee

Abstract This paper presents a novel method for printing thick silver electrodes with high fidelity using a rotogravure technique and high-viscosity silver ink. The widths and thicknesses of the printed electrodes were investigated with respect to the printing angle and printing speed. In addition, the use of a low-surface-energy polyethylene terephthalate substrate was found to decrease the ink transfer for printing angles of up to 60°, possibly because of the small adhesive force at the interface between the ink and substrate. We therefore employed substrates with higher surface energies, namely polyimide and treated polyimide, to enhance the ink transfer. A lower printing speed of 0.5 m/min and high viscosity of 15 Pa·s are required to obtain better functionality with a lower resistivity. However, using the proposed method, the fidelities of the printed patterns were achieved even with a high printing speed of 10.5 m/min using the high viscosity of 15 Pa·s, necessitating a subsequent sintering process. Therefore, the printed pattern was sintered in an oven at 350°C for 10 min. Patterned silver electrodes 1 m in length, 121 ± 2.2 μm in line width, 6.5 ± 2.2 μm in average thickness, and with a resultant resistivity of 9 μΩ·cm were achieved. The findings of this study confirm the potential of rotogravure printing for fabricating thick electrodes with high fidelity for flexible printed circuit boards with large areas.

Keywords Rotogravure, Thick film, Micropatterns, Flexible printed circuit boards, Aspect ratio

Electronic supplementary material The online version of this article (doi:10.1007/s11998-016-9844-y) contains supplementary material, which is available to authorized users.

Kee-Hyun Shin and Ho Anh Duc Nguyen have equally contributed to this work.

K.-H. Shin, H.A.D. Nguyen, D. Lee (✉)
Flexible Display Roll-to-Roll Research Center,
School of Mechanical Engineering, Konkuk University,
120 Neungdong-ro, Gwangjin-gu, Seoul 143-701, Korea
e-mail: djlee@konkuk.ac.kr

K.-H. Shin, D. Shin
TOBA Co., Ltd, 5F, Chung-San Bldg., Gwangnaru-ro 430,
Gwangjin-gu, Seoul 143-926, Korea

J. Park
Department of Mechanical Design and Production
Engineering, Konkuk University, 120 Neungdong-ro,
Gwangjin-gu, Seoul 143-701, Korea

Introduction

Over the last few years, roll-to-roll (R2R) printing has been found to offer a promising technology for fabricating low-cost large-area electronic circuits and devices on flexible plastic substrates.[1] Electronic devices such as organic light-emitting diodes and thin-film transistors have critical requirements, including minimum width,[2] precise control of the layer-to-layer register error,[3] and appropriate electrical conductivity.[4] The thickness of the printed layer generally determines the conductivity of the printed pattern. Although a line thickness as little as 50 nm, printed using ink containing silver nanoparticles as small as 5 nm, may afford sufficient conductivity for many printed electronics applications,[2] a method of printing thicker patterns with high current-carrying capabilities remains desirable for a wide range of electronic applications,[5] including solar cells.[6] One approach to addressing this issue is the fabrication of conductive lines with a small width and larger layer thickness.

Noncontact printing techniques such as electrohydrodynamic jet printing have been proposed for the fabrication of electrode lines with widths of 85 μm and thicknesses of 17.7 μm through multiple printing passes.[6] However, this strategy is inefficient because the printing speed is significantly slower compared to

other R2R printing techniques. Moreover, the multiple passes may increase the printed line width. For enhanced efficiency, screen printing has been used to fabricate a thick pattern with a width of 70 μm and a thickness of 4–5 μm. Nevertheless, there are limits to the extent to which screen printing can be integrated in a R2R manufacturing process.[7] In this paper, we propose a rotogravure printing method for the direct printing of thick electrodes with high fidelity.

The thickest printed electrode was arguably achieved by Kittilä et al.,[8] who developed a silicone-polymer direct gravure printing process for printing narrow conductor lines with widths of 40 μm and maximum thicknesses of 30 μm on a low-temperature cofired ceramic substrate. However, the silicone-polymer printing plate was only effective in the laboratory setting and not practical for industrial applications. Hrehorova et al.[9] investigated gravure printing and used conductive inks on a glass substrate to achieve a nominal line width of 50–500 μm. They showed that the printed pattern thicknesses and line width were determined by the printing angle and ink viscosity. In our previous work, we reported a rotogravure printing process that used silver (Ag) flakes and polyimide (PI) substrates with widths ranging between 30 and 120 μm.[10] However, despite the many previous works that have demonstrated the applicability of gravure printing to the fabrication of thicker patterns, few have achieved a thick film with high fidelity, as indicated by a high aspect ratio (AR), which is the ratio of the printed pattern's thickness to its width ($AR \geq 0.1$). Moreover, none of the previous works have considered the effects of printing parameters such as the printing speed on the profile of the printed patterns because their leveling times were sufficiently fast to achieve very smooth profiles, which nonetheless resulted in more spreading.

The rotogravure printing process has attracted much attention as a potentially low-cost method for fabricating printed electronics such as radio frequency identification tags,[11] sensors,[12] thin-film transistors,[13] and flexible displays.[14] This is because rotogravure overcomes the drawbacks of other R2R printing methods such as offset gravure and flexography, including the deformation of the engraved cylinder.[15,16] The rotogravure printing system consists of the driven engraved cylinder, an impression roller, and a doctor blade. A plastic substrate is stretched under an operating tension and moved through the entire system, including the engraved cylinder and impression roller. The printing roll is engraved to impress the desired patterns on the substrate. The ink is applied to the entire surface of the engraved cylinder, and the excess ink on the nonimage area is removed by the doctor blade. The remaining ink inside the engraved cell is subsequently brought into contact with the substrate. As the engraved cell separates from the substrate, the ink is split to produce filaments at the impression exit, P_{Exit}, with the filament rupture forming the print pattern on the substrate. Figure 1a shows a schematic of the general rotogravure printing process, which can be divided into four phases: (i) inking

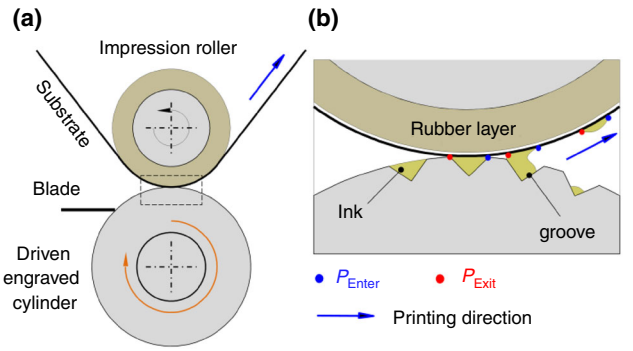

Fig. 1: Schematic representation of roll-to-roll gravure printing: (a) overall configuration and (b) detailed view of the contact point

phase at the ink supplier, (ii) doctoring phase at the doctor blade, (iii) printing phase in the contact area, and (iv) setting phase after the release of the ink from the cell. A detailed description of this process is available in the literature,[17] and a detailed view of the contact point is provided in Fig. 1b.

In the present study, we fabricated a thick Ag electrode for a flexible printed circuit board using rotogravure printing and high-viscosity inks. We initially investigated the effects of the viscosity, printing speed, and printing angles on the line width and thickness of the printed pattern. The effects of printing speed and ink viscosity on the resistivity of printed patterns was evaluated as well. We also experimented with various substrates to increase the amount of ink transfer. The optimal conditions thus identified were then used to print a thick electrode and its electrical resistance was measured along a length of 1 m.

Methods and materials

The experiments were performed on a commercial gravure printing machine (Sung An Machinery Co., Korea) in a class 1000 cleanroom environment (23°C and 50% relative humidity). The engraved cylinder was manufactured by Hyoungje Optics Co., Korea; it was made of steel, plated with copper, engraved with a laser, and finally plated with chromium. The groove-type engraved patterns were fabricated with a line width of 91.1 ± 0.5 μm and a nominal depth of 45 μm, as shown in Fig. 2a. The engraved pattern was designed in CAD as shown in Fig. 2b. This CAD model was used to fabricate the given pattern on the engraved cylinder. The image of the engraved pattern is located on the cylinder in line with the printing direction, as shown in Fig. 2b. To measure the thickness and line width of the printed pattern, the three points in the area defined as P1 were used. The area defined as P2 was designed to measure the functionality of the pattern in terms of its resistance and resistivity. Figure 2c magnifies Fig. 2b in the area of

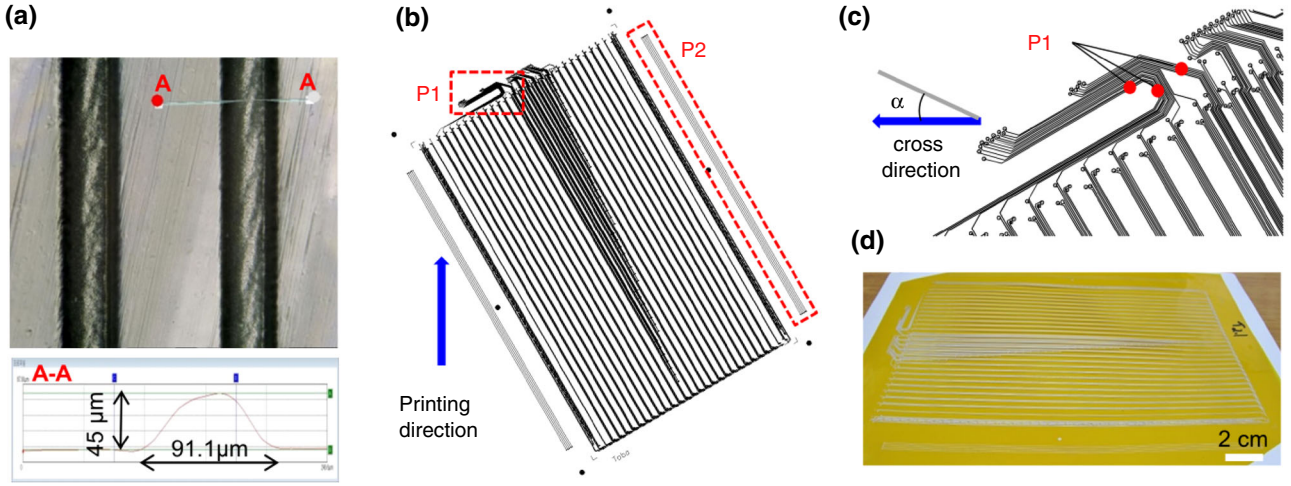

Fig. 2: Designed and printed micropatterns: (a) image and profile of the engraved cell on the engraved cylinder; (b) CAD image indicating the thickness measurement area (P1) and the resistance measurement length (P2); (c) magnified image at P1; and (d) pattern produced by rotogravure printing on a PI substrate

Table 1: Substrate and ink properties

Description	Parameter	Unit	Value
PET substrate	Width	mm	300
	Thickness	μm	100
	Surface energy	dyn/cm	42.6
PI substrate	Width	mm	300
	Thickness	μm	25
	Surface energy	dyn/cm	47.2
Treated PI substrate	Width	mm	300
	Thickness	μm	25
	Surface energy	dyn/cm	50.2
Ag ink	Viscosity	Pa·s	60
	Binder	wt%	8
	Solid content	wt%	60
	Flake size	μm	1.9–2.2

P1, showing the three points used to present the images of the printed patterns at the three printing angles. Finally, Fig. 2d shows a typical printed pattern produced by rotogravure printing on a PI substrate.

The selected substrates were a polyethylene terephthalate (PET) film (SH34, SK, Korea) with a width of 300 mm and caliper of 0.1 mm, and PI and surface-treated PI films with widths of 300 mm and calipers of 0.025 mm. The surface energies of the substrates were characterized by the static sessile drop method using distilled water. The contact angles (θ) were averaged over ten different measurements. For a given surface tension of water ($\gamma_{H_2O} = 72\,\mathrm{dyn/cm}$ at 25°C), the surface energy of the substrate (γ_{sub}) can be estimated using Newton's iterative method to solve the equation of state with an empirical constant, $\beta = 0.0001247$ (m/mN)^2, as shown in equation (1)[18]:

$$\cos\theta = -1 + 2\sqrt{\frac{\gamma_{sub}}{\gamma_{H_2O}}}e^{-\beta(\gamma_{sub}-\gamma_{H_2O})}. \quad (1)$$

The printing machine was operated with an impression pressure of 0.5 MPa and the doctor blade pressure of 3 MPa, and was supplied with flake-type Ag ink (Fine Paste Co., Korea) that contained epoxy (FPE-137) as a binder (8%) and 1.9–2.2 μm silver flakes with a solid content of 60 wt%. Three versions of the ink, with viscosities of approximately 5, 10, and 15 Pa·s, respectively, were prepared by diluting the unadulterated ink, with a viscosity of 60 Pa·s, with diethylene glycol dibutyl ether solvent. Table 1 summarizes the properties of the ink and the substrates used in this study. The rheological measurement was done at a shear rate of 50 rev/min, as measured by a rheometer (HAKKE Rheoscopes). Before reaching the dryer, the

Table 2: Traveling time and curing time of printed pattern

Printing speed (m/min)	L_{imp} (m)	t_{travel} (s)	L_{oven} (m)	t_{cure} (s)
0.5	1	120	5	600
5.5	1	10.9	5	54.5
10.5	1	5.7	5	28.6

printed patterns had to travel the 1-m distance between the impression and the dryer (L_{imp}) at room temperature. The printed pattern was cured on the PET and PI substrates in a 5-m-long oven (L_{oven}) at 80 and 150°C, respectively. The effects of the printing speed on the pattern fidelity, line width, and thickness were investigated by varying the printing speed between 0.5 and 10.5 m/min. As a result, the traveling time (t_{travel}) and the curing time (t_{cure}) could be estimated, as presented in Table 2. During the setting phase, the ink film was leveled on the substrate over time. The leveling time ($t_{leveling}$) can be calculated as follows[19]:

$$t_{leveling} = \frac{3}{16\pi^4}\frac{\mu_{ink}}{\gamma_{ink}}\frac{\lambda^4}{h^3}. \quad (2)$$

In equation (2), μ_{ink}, h, and λ are the ink viscosity, printed pattern thickness before drying, and filament fluctuation period, respectively. For a given μ_{ink} and γ_{ink}, the leveling time is proportional to λ^4/h^3.

The quality of the printed patterns was observed through an optical microscope (ECLIPSE LV100ND, Nikkon, Japan) positioned at P1, shown in Fig. 2b. The printability was defined as the ratio of the real printed area to the designed printed area

$$\text{Printability} = \left(1 - \frac{A_{Void}}{A_{Groove}}\right) \times 100. \quad (3)$$

In equation (3), A_{Void} and A_{Groove} denote the void area of the printed pattern and the top-view area of the engraved cell, respectively.

The thickness of the printed pattern was profiled using a surface profiler (NV 2000, Nano System, Korea). The three-dimensional data on the printed patterns was postprocessed using the OriginPro software. A magnetic tape was used to fix the sample to prevent undulation of the flexible substrate during the measurement process. For each printing trial, five samples were collected. The various locations of the measurement points in the area P1 are shown in Fig. 2c. The printing angle α was defined as the angle between the directions perpendicular to and in line with the printing direction. The electrical resistance (R) of the printed pattern was also measured under the optimal conditions using the two-point probe method by Probershoping. The measurement was done over L_p = 1 m, as indicated by P2 in Figs. 2b and 2d. The resistivity (ρ) was defined by

$$\rho = R\frac{w_P \cdot t_P}{L_P}, \quad (4)$$

where w_p and t_p are the line width and thickness of the printed pattern, respectively.

Results and discussion

As noted in the previous section, the ink was transferred to the substrate to form the pattern in the contact area. The formation of the two sides of the printed pattern edge is attributed to several mechanisms, including P_{Exit} and P_{Enter}, which are shown in Fig. 1b. P_{Exit} is located at the exiting side of the printed edge, at the points where the ink film exits the impression roller. The formation of P_{Exit} is a function of the ink viscosity and printing speed in the printing phase defined by the split pattern,[20,21] as well as in the doctoring phase such as the drag-out tail, streaks along the printing direction.[22] P_{Enter} is located at the entering side of the printed edge and is formed as the substrate is brought into contact with the ink and moves through the impression roller. Accordingly, the formation of P_{Enter} is a function of the relative speeds of the substrate and engraved cylinder. When the relative speeds of the substrate and engraved cylinder are the same, slippage will not occur, resulting in perfect print registration. When the engraved cylinder moves faster than the substrate, the ink is dragged forward along P_{Enter}. When the substrate moves faster than the engraved cylinder, the ink is dragged backward along P_{Exit}.[23]

It is believed that the substrate establishes the stick and slip zones as a function of the shear traction induced by the Hertzian contact stress of the impression roller and engraved cylinder.[24,25] In the stick zone, two conditions have to be fulfilled: (i) the rate of change of the strain on the substrate in the printing direction in the impression roller has to be zero; (ii) the friction forces cannot exceed the limiting value obeying Amontons's law.[25] Therefore, the slip area is a function of (i) substrate properties including thickness, Young modulus, and Poisson ratio; (ii) friction coefficient; and (iii) impression pressure, including impression force, rubber layer (thickness, Shore A), and contacting time (printing speed). Because the engraved cylinder was driven by a motor with a gear ratio of 30:1, the gear chatter-induced-slippage could be ignored.

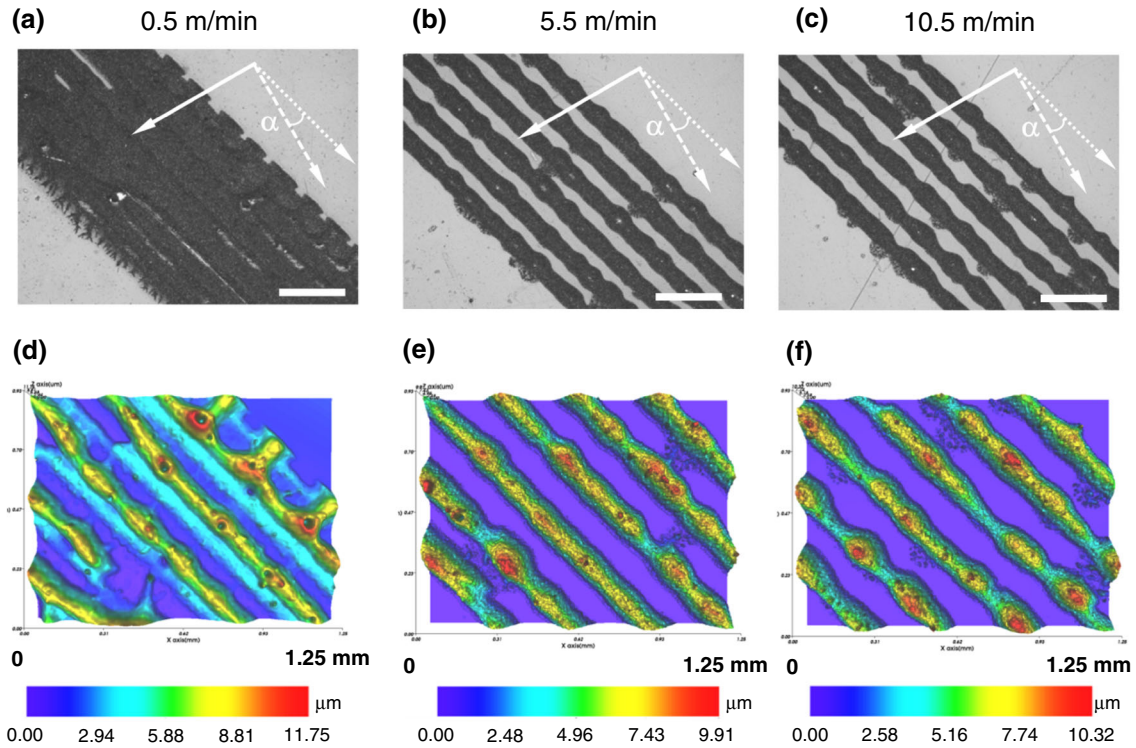

Fig. 3: Optical images (a–c) and 3D profiles (d–f) of silver line patterns printed by rotogravure printing using a printing angle of 15° on a PET substrate, ink with a viscosity of 5 Pa·s, and printing speeds of 0.5, 5.5, and 10.5 m/min, respectively. The dashed and continuous lines indicate the directions perpendicular to and in line with the printing direction, respectively. The yellow bars along the printed lines indicate the lengths over which the thickness was profiled. The white scale bar represents 500 μm (Color figure online)

Figure 3 shows the microscopic images and 3D profiles of the printed patterns for ink with a viscosity of 5 Pa·s and three printing speeds of 0.5, 5.5, and 10.5 m/min, respectively. All of the printed lines were observed to have moved in the printing direction over the same offset distance, thus producing a periodic rectangular residual ink mark on the entering side of the printed edges, P_{Enter} in Fig. 1b. This caused the ink to spread into the gaps as shown in Fig. 3a. A similar observation was made in a previous study for a very slow printing speed.[26] However, this spread can be mitigated by using a more viscous ink. Several explanations have been offered for this phenomenon: more viscous inks have a greater resistance to flow caused by the squeeze film action[9,27]; during the printing phase, the ink is doctored more faithfully at the edges of the line[22]; and more viscous inks exhibit greater inertia (higher density), which tends to limit spreading in the setting phase when the ink is leveled on substrate.[28] This is confirmed by comparing Figs. 3, 4, and 5, which show that the 5-Pa·s ink spread more than the 10- and 15-Pa·s inks. Furthermore, a more viscous ink was found to ensure greater fidelity to the printed pattern, as can be observed from Figs. 3, 4, and 5. These results are in good agreement with those of our previous work.[27] The line widths were also found to decrease with increasing viscosity, as shown in Fig. 6a.

As can be seen from Figs. 3, 4, and 5, the width and fidelity of the lines can be improved by increasing the printing speed. There was a significant reduction in the line width when the speed was increased from 0.5 to 5.5 m/min, and a more moderate reduction in the line width when the speed was further increased to 10.5 m/min. This observation is mainly attributed to the slipping behavior in the impression section, as discussed previously. The increase in the printing speed caused a decrease in the contact time. Furthermore, because of the viscoelastic characteristic of polymers like PET,[29] the rate of change of the strain on the substrate in the printing direction in the impression roller could be neglected as the contact time became smaller. Therefore, the no-slip condition of the impression roller could be established when the printing speed reached the critical value. As the printing speed reached 5.5 m/min, the printed patterns did not show any defect at P_{Enter}, thereby indicating a no-slip condition. From these results, we could claim that the critical value of the printing speed was smaller than 5.5 m/min in this study.

We believe that the smaller line widths obtained at high printing speeds of 5.5–10.5 m/min can be explained by the mechanism of the ink spread on the substrate in the printing phase. The spread is inhibited with increasing printing speed because of the reduced

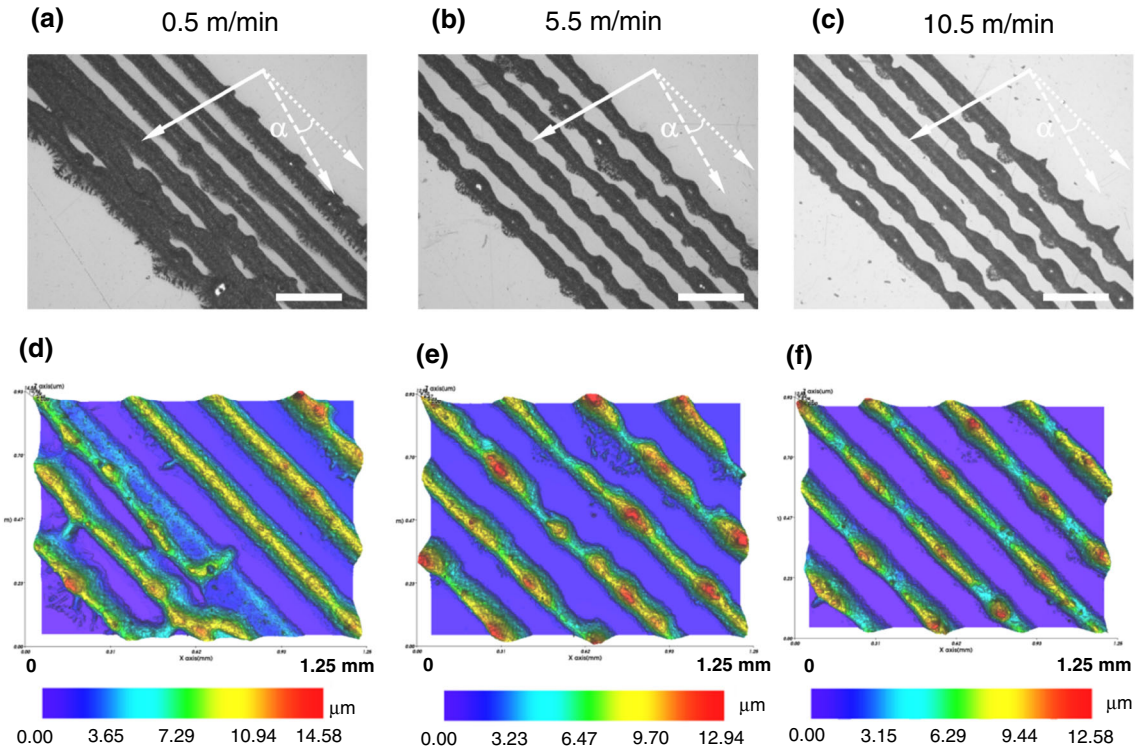

Fig. 4: Optical images (a–c) and 3D profiles (d–f) of silver line patterns printed by rotogravure printing using a printing angle of 15° on a PET substrate, ink with a viscosity of 10 Pa·s, and printing speeds of 0.5, 5.5, and 10.5 m/min, respectively. The dashed and continuous lines indicate the directions perpendicular to and in line with the printing direction, respectively. The yellow bars along the printed lines indicate the lengths over which the thickness was profiled. The white scale bar represents 500 μm (Color figure online)

dwelling time of the ink and substrate, leading to a reduced momentum transferred to the ink.[27] In addition, the effect of the printing speed was found to be most significant for the 5-Pa·s ink, followed by the 10-Pa·s ink, and then the 15-Pa·s ink, as shown in Fig. 6a.

It is evident that the size and distribution of the split pattern formed immediately after the impression exit are functions of the ink viscosity and printing speed.[20,21] The filaments were formed from the split patterns, and ruptured by the rotation of the printing roller. The filaments recoiled onto the substrate and created a thick nonuniform printed pattern, which was leveled over time by the surface tension and gravitational forces.[30] The leveling time is a function of the ink viscosity, print thickness, and surface tension of the ink, as shown in equation (2). Furthermore, the printed pattern was continuously exposed to hot air during the curing process, and this rapidly increased the ink viscosity. As soon as the solvent evaporated completely into the hot air, the leveling process ceased. This was because of the high surface roughness of the printed pattern when the leveling time extended beyond the solvent evaporation time.

Figures 3, 4, and 5 also show the effect of the printing speed and ink viscosity on the profile of the printed pattern. The ink with the lowest viscosity of 5 Pa·s formed the smoothest surface, as indicated by the fewer peaks, followed by the 10- and 15-Pa·s inks, respectively, as shown in Fig. 6c. Furthermore, the average thicknesses of the printed patterns were found to increase with increasing ink viscosity. This is mainly attributed to the cross-sectional slump of the printed patterns on both sides due to gravity, resulting in reduced thickness and increased line width, as shown in Fig. 6b. This corroborates the leveling effect of the ink viscosity on the printed pattern, as discussed earlier. Similar results have been previously obtained.[9,28]

An increase in the printing speed increased the formation of the split pattern, decreased the curing time required for the complete evaporation of the solvent, and simultaneously decreased the traveling time, as shown in Table 2. In addition, the increase in speed also increased the elongation strain rate on the film at the rear end of the impression roller (P_{Exit}), and this influenced the film splitting, leading to an altered morphology of the printed patterns.[31] Therefore, a higher speed increased the number of peaks for all the inks of differing viscosities, as can be observed from Figs. 3, 4, 5, and 6c. However, for a printing speed of 0.5 m/min, the number of peaks for the low ink viscosity of 5 Pa·s was higher than those for the other two ink viscosities of 10 and 15 Pa·s, contrary to previous reports. As the ink viscosity increased, the surface roughness of the printed pattern increased.[31,32]

Table 3: Results of rotogravure compared with screen printing

Printed pattern	Line width w_P (μm)	Thickness t_P (μm)	Thickness L_P (m)	Resistance R (Ω)	Resistivity ρ (μΩ cm)	Printed line/Ag bulk
Gravure printing	121	6.5	1000	180	9.0	14
Screen printing	100	3	1000	1100[a]	33.0	21
Screen printing	100	6	1000	883[a]	53.0	33

Resistivity of Ag bulk is 1.6 μΩ.cm

[a] Reference 38

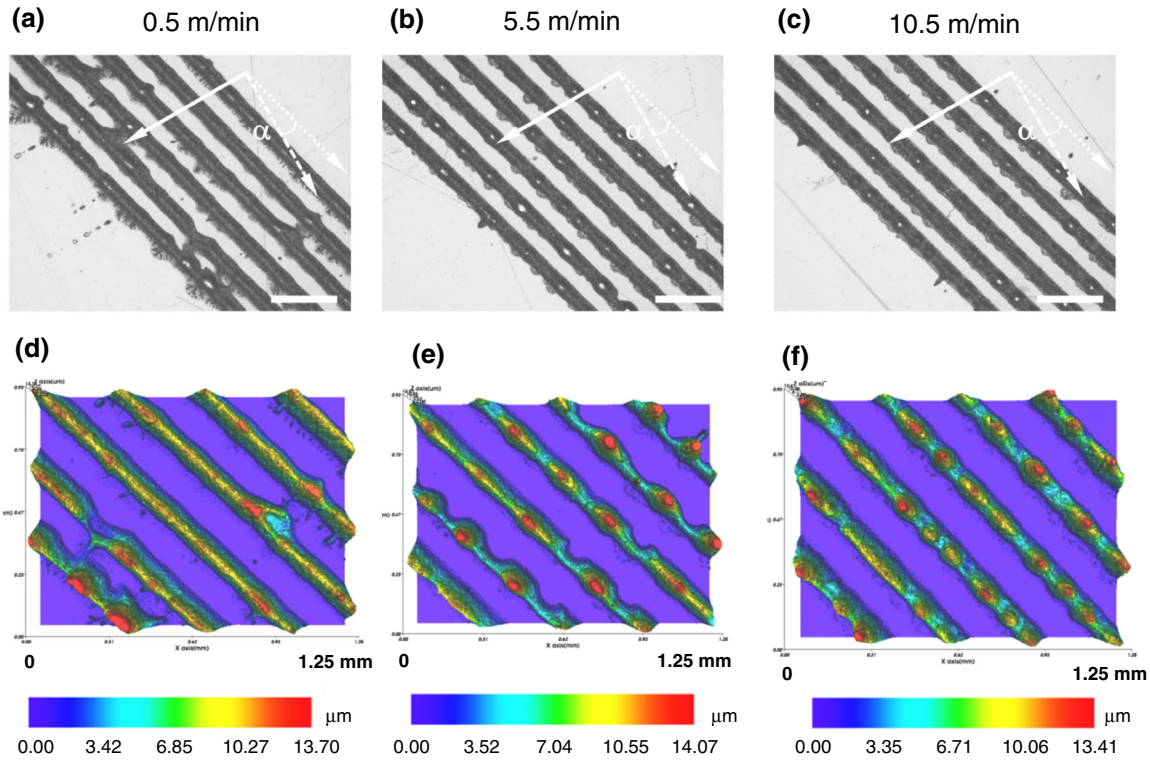

Fig. 5: Optical images (a–c) and 3D profiles (d–f) of silver line patterns printed by rotogravure printing using a printing angle of 15° on a PET substrate, ink with a viscosity of 15 Pa·s, and printing speeds of 0.5, 5.5, and 10.5 m/min, respectively. The dashed and continuous lines indicate the directions perpendicular to and in line with the printing direction, respectively. The yellow bars along the printed lines indicate the lengths over which the thickness was profiled. The white scale bar represents 500 μm (Color figure online)

This could be due to the slipping behavior of the substrate in the contact area for a low printing speed of 0.5 m/min, as discussed earlier and illustrated in Figs. 3d, 4d, and 5d. The slippage of the substrate causes the distortion of the printed pattern geometry shown in the optical images and 3D profiles, resulting in the abovementioned anomaly.

Figure 7 shows the resistivity of the printed pattern as a function of speed and viscosity for a printing angle of 30°. The resistivities of the printed patterns decreased when using higher viscosity ink and lower printing speed. This is because the amount of Ag solid is expected to increase with the thicker printed patterns. In addition, using the higher viscosity ink leads to a greater thickness of the printed pattern, as shown in Fig. 6b. This effect of ink viscosity on the resistivity of the printed pattern is in good agreement with other studies.[33] At such a low printing speed of 0.5 m/min, the resistivity of the printed pattern was low. This is due mainly to the fact that a t_{cure} of 600 s is long enough to dry out more solvent from the printed patterns, compared to other cases with a smaller t_{cure} at a higher printing speed (see Table 2).

The results presented in the previous section show that the high-viscosity ink (15 Pa·s) afforded high fidelity of the printed pattern, represented by the narrow line width of 132.2 ± 6.7 μm and the high maximum thickness of 10.92 μm. Accordingly, this ink

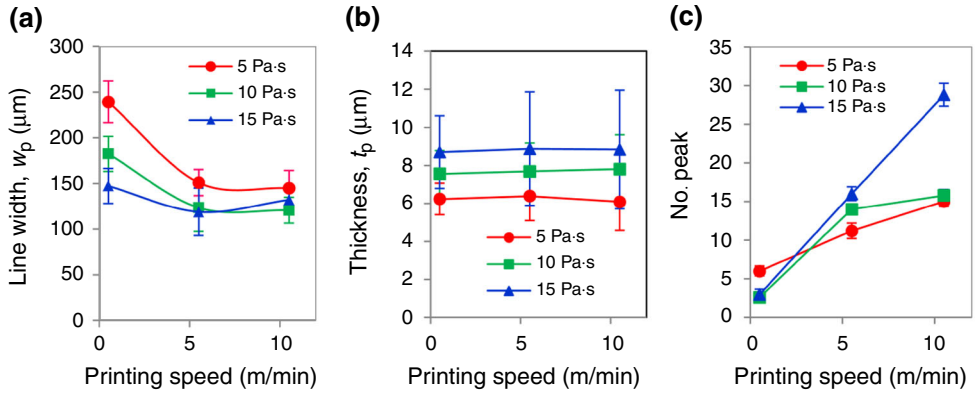

Fig. 6: Printed line pattern: (a) measured width; (b) measured thickness; and (c) number of peaks with respect to the printing speed and ink viscosity for a printing angle of 15°

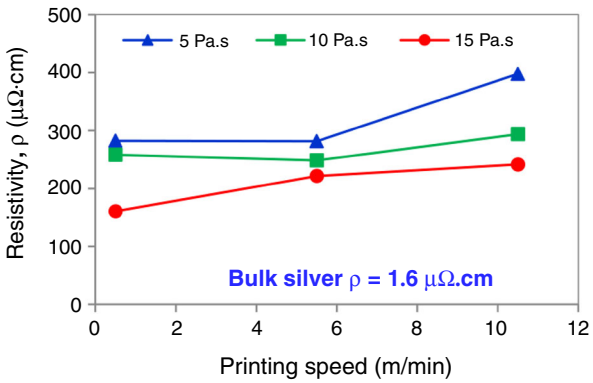

Fig. 7: Resistances of the printed line patterns for a printing angle of 30° as a function of ink viscosity and printing speed

and a PET substrate were used to investigate the effect of the printing angle α on the printed pattern and the printability for a printing speed of 10.5 m/min. Figures 8g and 8h show the effect of the printing angle on the line width and thickness profile. It has been previously reported that the printed line width increases with a decreasing printing angle.[9] However, the present investigation revealed that the line widths decreased slightly from 132.2 ± 6.7 to 131.3 ± 5.3 μm as α was increased from 15° to 30°, and rapidly decreased to 92.6 ± 32.7 μm when α was further increased to 60°, as shown in Fig. 8g. Similar behavior has previously been attributed to the orientation of the cell's sidewalls, whereby the decrease in α results in greater spreading and a larger line width.[34] Figure 8h shows that the thickness of the printed pattern was independent of α. The decrease in the average thickness of the printed patterns when α = 60° is because the void area causes greater thickness variation, as indicated by the higher standard deviation.

Figures 8a–8c compare the optical images of the printed pattern for α values of 15°, 30°, and 60°. The printabilities and printed line widths for α = 15° and 30° seem to be similar and interestingly better than those for α = 60°. The printability of the gravure printing method can be attributed to the adhesive force at the interface between the ink and the substrate. This interfacial force can increase by increasing either the interfacial contact area or the work of the adhesive, i.e., the surface energy of the substrate.[35] The interfacial contact area (A) is a function of the foot print of the impression roller (b) and the printing angle (α).[27,34,36] Because the length L_P of the printed pattern shown in Fig. 2 is much larger than its foot print (b is approximately 5 mm), the interfacial area can be estimated using the following equation, derived from Fig. S1 in Supporting Information:

$$A_{IS} = \begin{cases} w_P L_P & 0° \le \alpha \le \arctan(b/L_P) \\ w_P(b/\sin\alpha) & \arctan(b/L_P) < \alpha \le 90° \end{cases}. \quad (5)$$

It can be seen from the above equation that A_{IS} decreases with increasing α, resulting in reduction of the printability for printing angles of up to 60°. The effects of α on the thickness and line width are thus similar, which can also be observed from Figs. 9a and 9b. Because of the good printabilities for printing angles of 15° and 30°, the corresponding thickness profiles are almost the same. However, because of the poorer printability for a printing angle of 60°, the thickness profile contains some voids (i.e., areas of zero thickness), as shown in Fig. 8f.

Although Fig. 8i shows that the printability for α = 60° was the lowest, the narrower line produced by a larger printing angle is advantageous for achieving a high AR for a given pattern thickness, as mentioned earlier. An alternative means of increasing the printability is the use of a substrate with a higher surface energy.[37] Figure 9 compares the optical images of lines printed on various substrates using α = 60° and a printing speed of 10.5 m/min. The surface energies for the three substrates (PET, PI, and treated PI) were characterized by the contact angle of a sessile drop of distilled water, as illustrated in the insets in Figs. 9a–9c.

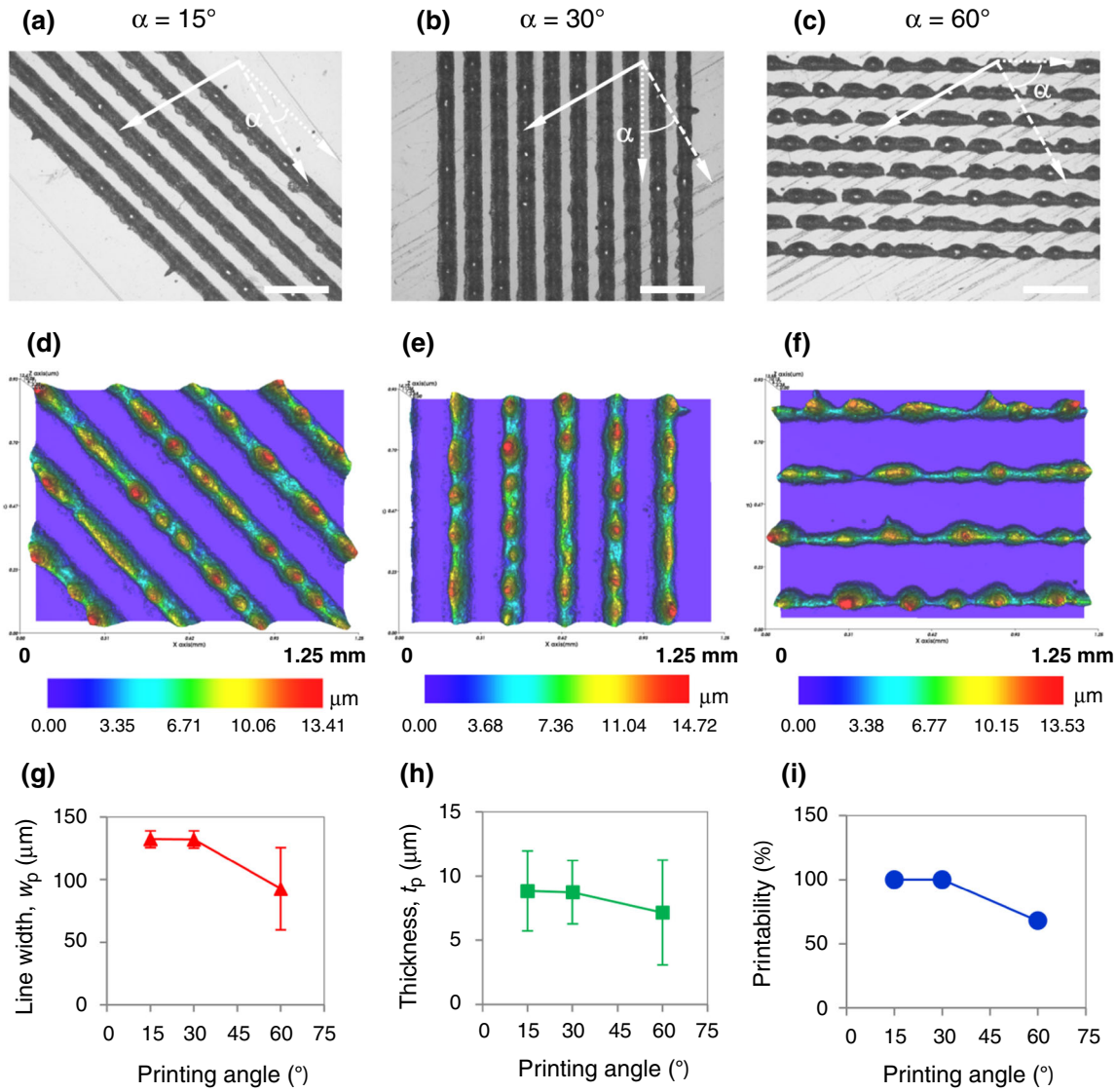

Fig. 8: Optical images (a–c); 3D-profiles (d–f); and line widths, thicknesses, and printabilities (g–i) of the line patterns printed by rotogravure printing using a printing speed of 10.5 m/min, a PET substrate, an ink with a viscosity of 15 Pa·s, and printing angles of (a) 15°, (b) 30°, and (c) 60°. The dashed and continuous lines indicate directions perpendicular to and in line with the printing direction, respectively. The scale bar represents 500 μm

From Fig. 9d, it can be seen that the printability increases with increasing surface energy of the substrate. Among the three substrates, the treated PI has the highest surface energy of 50.2 dyn/cm, and hence the best printability using the 15-Pa·s ink, $\alpha = 60°$, and a printing speed of 10.5 m/min, as shown in Fig. 9c.

The optimal conditions for printing were found to be a printing speed of 10.5 m/min, ink viscosity of 15 Pa·s, printing angle of 60°, and treated PI substrate. At this high printing speed of 10.5 m/min at which t_{cure} = 28.6 s, the resistivity of the printed pattern achieved the high value shown in Fig. 7. Therefore, a subsequent sintering process was necessitated, applied only to the optimal PI substrate. The printed pattern was sintered in an oven at 350°C for 10 min. The obtained line width was 121 ± 2.2 μm, and the average thickness was 6.5 ± 2.2 μm. The resistance reached 183.3 ± 1.1 Ω along a length of 1 m. We compared these results with our previous study using the screen printing method,[38] in which the printed pattern achieved the resistivity of 9 μΩ·cm, approximately 14× Ag bulk. Although the resistivity of the printed pattern attained a value of 3.61 μΩ·cm, which is approximately 2× Ag bulk when using silver nanoparticle ink,[39] the screen printing method still has limitations, such as the high cost of silver nanoparticle ink and an unacceptably short pattern length (L_P = 1.4 mm) for large-area flexible printed circuit boards. The rotogravure results are much better than those obtained using the conventional screen printing process, as shown in Table 3. Our work is still more advantageous because of the following reasons: (i) the lower cost of the flake

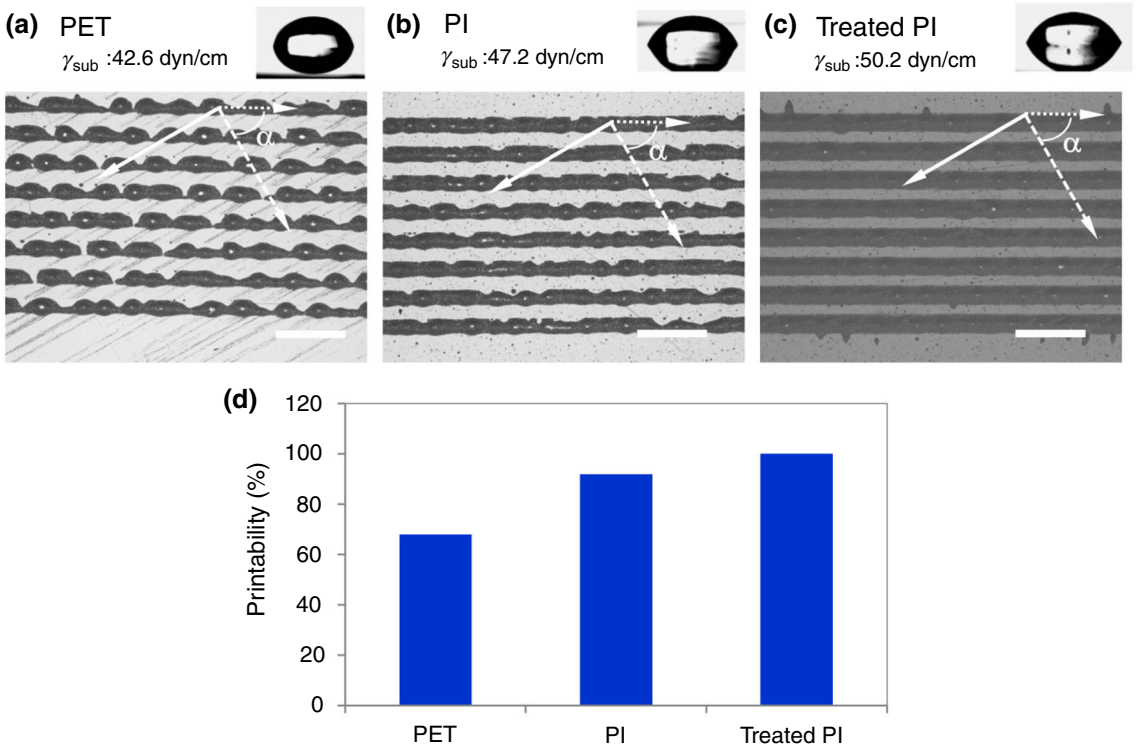

Fig. 9: Optical images of the line patterns printed by rotogravure printing using a printing angle of 60° and printing speed of 10.5 m/min on different substrates. The dashed and continuous lines indicate the directions perpendicular to and in line with the printing directions, respectively. The scale bar represents 500 μm

material used for the ink; and (ii) the larger printed area for flexible printed circuit boards at the meter scale. Therefore, this work demonstrates the feasibility of using rotogravure printing to fabricate printed electrodes for flexible printed circuit boards, particularly on an industrial scale.

Conclusions

We have investigated the application of rotogravure printing to the fabrication of silver electrodes on a plastic substrate for use in flexible printed circuit boards. Three types of silver inks with differing viscosities were used, and it was found that a higher viscosity produced narrower and thicker printed lines. The printing speed was also observed to significantly affect the fidelity and profile of the printed patterns. A printing speed that is too low causes the substrate to slip relative to the engraved cylinder, resulting in distortion of the printed pattern. A faster printing speed leading to a shorter contact time inhibits the slippage. It was also observed that the printing angle, which is the angle between the engraved pattern and the cross printing direction, affected the printability. The printability could also be enhanced by using a substrate with a higher surface energy. The resistivity of the printed pattern is lower when printing at low speed with high viscosity of ink. While curing requirements such as a long curing time and high temperature could hinder the application of the proposed rotogravure process, roll-to-roll infrared drying and sintering processes could be a solution to this problem. The findings of this study confirm the feasibility of using rotogravure printing for high-throughput fabrication of large-area flexible printed circuit boards. A detailed investigation of the slippage phenomenon of the substrate on the engraved cylinder can be conducted experimentally and/or with computational simulations to provide further insight.

Acknowledgments This study was funded by a Konkuk University research support program. Further support was provided by the Global Leading Technology Program funded by the Ministry of Trade, Industry and Energy (10042537) and by the Leading Foreign Research Institute Recruitment Program through the National Research Foundation of Korea (NRF) funded by the Ministry of Science, ICT & Future Planning (MSIP) (Grant Number: 2010-00525), Republic of Korea.

References

1. Roth, B, Søndergaard, RR, Krebs, FC, "7—Roll-to-Roll Printing and Coating Techniques for Manufacturing Large-

Area Flexible Organic Electronics.'' In: Logothetidis, S (ed.) *Handbook of Flexible Organic Electronics*, pp. 171–197. Woodhead Publishing, Oxford, 2015
2. Kang, H, Kitsomboonloha, R, Jang, J, Subramanian, V, ''High-Performance Printed Transistors Realized Using Femtoliter Gravure-Printed Sub-10 μm Metallic Nanoparticle Patterns and Highly Uniform Polymer Dielectric and Semiconductor Layers.'' *Adv. Mater.*, **24** (22) 3065–3069 (2012)
3. Kang, H, Lee, C, Shin, K, ''Modeling and Compensation of the Machine Directional Register in Roll-to-Roll Printing.'' *Control Eng. Pract.*, **21** (5) 645–654 (2013)
4. Nguyen, HAD, Hoang, N, Shin, K-H, Lee, S, ''Statistical Analysis on the Effect of Calendering Process Parameters on the Geometry and Conductivity of Printed Patterns.'' *Robot Comput. Integr. Manuf.*, **29** (2) 424–430 (2013)
5. Yamamoto, T, Numakura, D, ''Advanced Fine-Line Thick-Film Conductors with High Conductivity and Soldering Capability Built by Screen-Printing.'' *Trans. Jpn. Inst. Electron. Packag.*, **2** (1) 40–45 (2009)
6. Jang, Y, Hartarto Tambunan, I, Tak, H, Dat Nguyen, V, Kang, T, Byun, D, ''Non-contact Printing of High Aspect Ratio Ag Electrodes for Polycrystalline Silicone Solar Cell with Electrohydrodynamic Jet Printing.'' *Appl. Phys. Lett.*, **102** (12) 123901 (2013)
7. Tsunomura, Y, Yoshimine, Y, Taguchi, M, Baba, T, Kinoshita, T, Kanno, H, Sakata, H, Maruyama, E, Tanaka, M, ''Twenty-Two Percent Efficiency HIT Solar Cell.'' *Sol. Energy Mater. Sol. Cells*, **93** (6–7) 670–673 (2009)
8. Kittila, M, Hagberg, J, Jakku, E, Leppavuori, S, ''Direct Gravure Printing (DGP) Method for Printing Fine-Line Electrical Circuits on Ceramics.'' *IEEE Trans. Electron. Packag. Manuf.*, **27** (2) 109–114 (2004)
9. Hrehorova, E, Rebros, M, Pekarovicova, A, Bazuin, B, Ranganathan, A, Garner, S, Merz, G, Tosch, J, Boudreau, R, ''Gravure Printing of Conductive Inks on Glass Substrates for Applications in Printed Electronics.'' *J. Disp. Technol.*, **7** (6) 318–324 (2011)
10. Park, J, Nguyen, HAD, Park, S, Lee, J, Kim, B, Lee, D, ''Roll-to-Roll Gravure Printed Silver Patterns to Guarantee Printability and Functionality for Mass Production.'' *Curr. Appl. Phys.*, **15** (3) 367–376 (2015)
11. Minhun, J, Jaeyoung, K, Jinsoo, N, Namsoo, L, Chaemin, L, Gwangyong, L, Junseok, K, Hwiwon, K, Kyunghwan, J, Leonard, AD, Tour, JM, Gyoujin, C, ''All-Printed and Roll-to-Roll-Printable 13.56-MHz-Operated 1-bit RF Tag on Plastic Foils.'' *IEEE Trans. Electron. Dev.*, **57** (3) 571–580 (2010)
12. Nam, D, Park, J, Park, S, Min, Y, Noh, Y, Lee, D, ''High-Density Hydrothermal Growth of Zinc-Oxide Nanowires Using Printed Resistive Heater.'' *Mater. Lett.*, **153** 29–32 (2015)
13. Lau, PH, Takei, K, Wang, C, Ju, Y, Kim, J, Yu, Z, Takahashi, T, Cho, G, Javey, A, ''Fully Printed, High Performance Carbon Nanotube Thin-Film Transistors on Flexible Substrates.'' *Nano Lett.*, **13** (8) 3864–3869 (2013)
14. Cheng-Yao, L, Huttunen, OH, Hiitola-Keinanen, J, Petaja, J, Fujita, H, Toshiyoshi, H, ''MEMS-Controlled Paper-Like Transmissive Flexible Display.'' *J. Microelectromech. Syst.*, **19** (2) 410–418 (2010)
15. Yusof, MS, Claypole, TC, Gethin, DT, Zaidi, AMA, ''Application of Finite Elements on Non-Linear Deformation of Flexographic Photopolymer Printing Plate.'' *Proceedings of the World Congress on Engineering*, Lecture Notes in Engineering and Computer Science, 2008
16. Kang, D, Lee, E, Kim, H, Choi, Y-M, Lee, S, Kim, I, Yoon, D, Jo, J, Kim, B, Lee, T-M, ''Investigation on Synchronization of the Offset Printing Process for Fine Patterning and Precision Overlay.'' *J. Appl. Phys.*, **115** (23) 234908 (2014)
17. Nguyen, HAD, Lee, J, Kim, CH, Shin, K-H, Lee, D, ''An Approach for Controlling Printed Line-Width in High Resolution Roll-to-Roll Gravure Printing.'' *J. Micromech. Microeng.*, **23** (9) 095010 (2013)
18. Kwok, DY, Lam, CNC, Li, A, Zhu, K, Wu, R, Neumann, AW, ''Low-Rate Dynamic Contact Angles on Polystyrene and the Determination of Solid Surface Tensions.'' *Polym. Eng. Sci.*, **38** (10) 1675–1684 (1998)
19. Hernandez-Sosa, G, Bornemann, N, Ringle, I, Agari, M, Dörsam, E, Mechau, N, Lemmer, U, ''Rheological and Drying Considerations for Uniformly Gravure-Printed Layers: Towards Large-Area Flexible Organic Light-Emitting Diodes.'' *Adv. Funct. Mater.*, **23** (25) 3164–3171 (2013)
20. Miller, JC, Myers, RR, ''A Photographic Study of Liquid Flow in a Roll Nip.'' *Trans. Soc. Rheol.*, **2** (1) 77–93 (1958)
21. Myers, RR, Miller, JC, Zettlemoyer, AC, ''The Splitting of Thin Liquid Films. Kinematics.'' *J. Colloid Sci.*, **14** (3) 287–299 (1959)
22. Kitsomboonloha, R, Subramanian, V, ''Lubrication-Related Residue as a Fundamental Process Scaling Limit to Gravure Printed Electronics.'' *Langmuir*, **30** (12) 3612–3624 (2014)
23. Kim, S, Sung, HJ, ''Effect of Printing Parameters on Gravure Patterning with Conductive Silver Ink.'' *J. Micromech. Microeng.*, **25** (4) 045004 (2015)
24. Tomimatsu, M, Yamaura, H, Ono, K, ''Analysis of Surface Strain of a Paper in a Nip Roller Mechanics with a Rubber-layered Roller and a Steel Roller.'' *Trans. Jpn. Soc. Mech. Eng. Ser. C*, **71** (712) 3517–3524 (2005)
25. Welp, EG, Guldenburg, B, ''Analysis of the Kinematic and Dynamic Process During Winding Based on a Systematology of Models for Winding Mechanics.'' *Proceedings of the 4th International Conference on Web Handling*, Stillwater, Oklahoma, 1997
26. Yoon, D, Lee, S-H, ''Precision Gravure Printing of Conductive Ink on Flexible Substrate for Printed Electronics.'' *Proceedings of the* ASME 2012 International Mechanical Engineering Congress and Exposition, Houston, Texas, November 9–15, 2012
27. Nguyen, HAD, Shin, K-H, Lee, D, ''Effect of Process Parameters on Fidelity of Printed Line Width in High Resolution Roll-to-Roll Gravure Printing.'' *Jpn. J. Appl. Phys.*, **53** (5S3) 05HC04 (2014)
28. Kewish, RW, Wilcock, DF, ''Flow Properties of Paints Leveling.'' *Industrial & Engineering Chemistry*, **31** (1) 76–83 (1939)
29. Murayama, T, Dumbleton, JH, Williams, ML, ''Viscoelasticity of Oriented Poly(ethylene terephthalate).'' *J. Polym. Sci. A-2*, **6** (4) 787–793 (1968)
30. Orchard, SE, ''On Surface Levelling in Viscous Liquids and Gels.'' *Appl. Sci. Res.*, **11** (4–6) 451–464 (1963)
31. Toshiharu, E, Manabu, T, Fumihiko, O, Saburo, H, Hitoshi, N, Koji, T, Kazunori, K, ''Mechanisms of Print Gloss Development.'' *Proceedings of 2000 TAPPI International Printing & Graphic Arts Conference*, Atlanta, 2000
32. Hayashi, T, Mori, T, Amari, T, ''Dynamics of Transfer and Splitting of Emulsified Ink.'' *J. Print. Sci. Technol.*, **30** (1) 28–33 (1993)
33. Noh, J, Yeom, D, Lim, C, Cha, H, Han, J, Junseok, K, Park, Y, Subramanian, V, Cho, G, ''Scalability of Roll-to-Roll Gravure-Printed Electrodes on Plastic Foils.'' *IEEE Trans. Electron. Packag. Manuf.*, **33** (4) 275–283 (2010)

34. Higgins, SG, Boughey, FL, Hills, R, Steinke, JHG, Muir, BVO, Campbell, AJ, ''Quantitative Analysis and Optimization of Gravure Printed Metal Ink, Dielectric, and Organic Semiconductor Films.'' *ACS Appl. Mater. Interfaces*, **7** (9) 5045–5050 (2015)
35. Nguyen, HAD, Lee, C, Shin, K-H, Lee, D, ''An Investigation of the Ink-Transfer Mechanism During the Printing Phase of High-Resolution Roll-to-Roll Gravure Printing.'' *IEEE Trans. Compon. Packag. Manuf. Technol.*, **5** (10) 1516–1524 (2015)
36. Nguyen, HAD, Shin, K, Lee, C, ''Effect of Nip Force on Ink Transfer in High Resolution Roll-to-Roll Printing.'' *Int. J. Precis. Eng. Manuf.*, **16** (3) 517–523 (2015)
37. Morsy, FA, Elsayad, SY, Bakry, A, Eid, MA, ''Surface Properties and Printability of Polypropylene Film Treated by an Air Dielectric Barrier Discharge Plasma.'' *Surf. Coat. Int. B*, **89** (1) 49–55 (2006)
38. Choi, EK, Park, J, Kim, BS, Lee, D, ''Fabrication of Electrodes and Near-Field Communication Tags Based on Screen Printing of Silver Seed Patterns and Copper Electroless Plating.'' *Int. J. Precis. Eng. Manuf.*, **16** (10) 2199–2204 (2015)
39. Mahajan, A, Frisbie, CD, Francis, LF, ''Optimization of Aerosol Jet Printing for High-Resolution, High-Aspect Ratio Silver Lines.'' *ACS Appl. Mater. Interfaces*, **5** (11) 4856–4864 (2013)